Dynamic and Coordinated Control of a DC Microgrid Integrated with High-Temperature PEM Fuel Cell and High-Percentage of Renewable Energy

Xie, Peilin; Tan, Sen; Sahlin, Simon Lennart; Liso, Vincenzo

Published in:
2024 IEEE 10th International Power Electronics and Motion Control Conference (IPEMC2024-ECCE Asia)

DOI (link to publication from Publisher):
10.1109/IPEMC-ECCEAsia60879.2024.10567624

Publication date:
2024

Document Version
Accepted author manuscript, peer reviewed version

Dynamic and Coordinated Control of a DC Microgrid Integrated with High-Temperature PEM Fuel Cell and High-Percentage of Renewable Energy

1st Peilin Xie
Energy Department
Aalborg University
Denmark
pxi@energy.aau.dk

2nd Sen Tan
Energy Department
Aalborg University
Denmark
sta@energy.aau.dk

3rd Simon Lennart Sahlin
Energy Department
Aalborg University
Denmark
sls@energy.aau.dk

4th Vincenzo Liso
Energy Department
Aalborg University
Denmark
vli@energy.aau.dk

***Abstract*—The increasing demand for decarbonization has accelerated the adoption of renewable energy and the reduction of the reliance on conventional grid. This paper explores the modeling, controlling, and management of a DC microgrid, which predominantly relies on renewable energy and e-fuels for its normal operations. The studied DC microgrid integrates photovoltaic (PV), methanol-reformed high-temperature Proton Exchange Membrane Fuel Cell (HT-PEMFC), and batteries. The primary focus of this study is to coordinate the diverse energy resources, ensuring dynamic responsiveness to load demands while maintaining high operational efficiency. To achieve this, system models are developed and a decentralized control framework is established for each energy sector converter. This framework, noted for its simplicity, ensures optimal integration, efficient operation, and smooth transitions between operational modes, enabling the microgrid to operate autonomously and with human oversight. Through simulation studies, we demonstrate the effectiveness and coordinated operation of the proposed system. The simplicity of the controlling and management system showcases the potential for easy integration with advanced and high-level energy management system, and thereby has the practicality across wide ranges of microgrid applications.**

***Index Terms*—Fuel cell, DC Microgrids, power management system.**

I. Introduction

In the pursuit of sustainable energy solutions, there has been a growing interest in the integration of diverse renewable energy sources, including water, wind, solar, and bio-fuel or biomass. PV panels, wind turbines, and fuel cells have emerged as critical components in shaping the next-generation energy system. The DC microgrid, due to its advantages such as enhanced efficiency, reduced transmission losses, and seamless integration capabilities, is becoming the key solution for the effective integration of these renewable energy sources [1].

PEM fuel cells, having undergone comprehensive study and evaluation, are recognized as highly advantageous energy conversion systems owing to their remarkable efficiency, extended lifespan, compact dimensions, and zero CO2 emissions. Nevertheless, it is noteworthy that they exhibit a comparatively slow response to fluctuations in power demand.

While the adoption of DC microgrids offers flexibility and convenience for the hybrid operation of different energy sources, achieving efficient and reliable cooperation among them still requires advanced control strategies. Previous research in this area has proposed various control strategies, often categorized into three layers [2]: the primary layer, which focuses on inverter control for preliminary power sharing and typically consists of droop control, PI control [3]; the secondary layer typically refers to the secondary load sharing for the enhancement of power quality [4]; and the tertiary layer, involving complex decision-making processes, such as energy management system (EMS), to achieve objectives such as operational fuel efficiency, cost reduction, low carbon emissions, and extended component lifespan [5]. There have been numerous papers addressing various microgrid types and making advancements in controller development within each category. However, for the efficient and reliable operation of real-world micorgid, collaboration across all these three layers is required. In addition to it, changes in power system topology bring out significant adjustments to control strategies. Consequently, a case-by-case design becomes necessary, thereby increasing the complexity of controller development and limiting the scalability of microgrids.

This paper addresses this research gap by introducing a simplified DC microgrid structure and developing a dynamic decentralized control framework for it. The primary focus lies in ensuring stable and efficient microgrid operation under load variations and seamless operational mode transition for each energy sector in the absence of tertiary control. The proposed control method is simply in structure and can be easily adopted for different microgrid applications and offers an easily integrable potential for advanced EMS, thereby facilitating a more comprehensive and sustainable microgrid

This work was supported by FC-COGEN (223853).

operation. This digest contains only part of the research content. Details in regards to the system modeling, power and energy management system designing will be presented in the full text.

II. System Description and Modeling

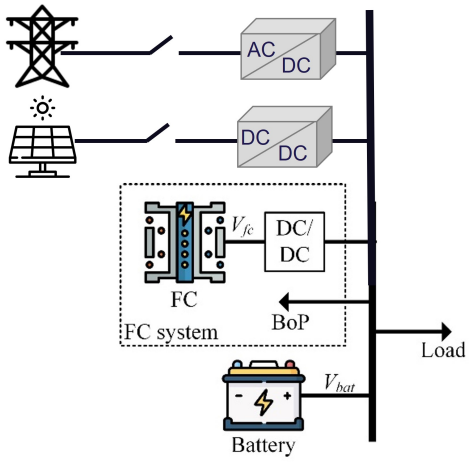

Fig. 1. Microgrid structure.

A. System Structure

The general structure of the studied system is as Fig. 1. The grid is connected to the DC bus through an AC/DC converter, which allows the microgrid to operate in both grid-connected and islanded modes. To reduce the dependence on the grid, renewable energy sources are adopted. The PV turbine operates in Maximum Power Point Tracking (MPPT) mode through a DC/DC converter to maximize the usage of available renewable energy. To compensate for the intermittent nature of renewables, a 5kW methanol reformed HT-PEMFC system is connected to the DC bus via a DC/DC converter. The PEMFC system model includes model for the FC stack as well as the BoP components. Lastly, a battery is adopted and is directly linked to the DC bus.

B. Methanol Reformed HT-PEMFC system model

To effectively capture the transient dynamics while maintaining a balance between simplicity and computational efficiency, a simplified yet dynamic model is developed for the methanol reformed HT-PEM fuel cell system. The overall structure of it is presented in Fig. 2.

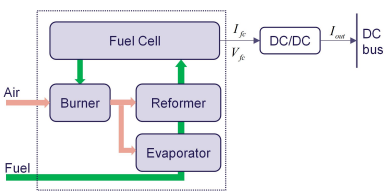

Fig. 2. General structure of a methanol reforming HT-PEMFC system

The methanol reformed fuel cell system utilizes a fuel mix comprising 60% methanol and 40% deionized water. Initially, the mixture is heated to a gseous state upon passing through an evaporator. Following this, the vaporized fuel enters the reformer where these three reactions takes places [6].

Methanol steam reforming reaction:

$$CH_3OH + H_2O \leftrightarrow CO_2 + 3H_2 \qquad \Delta = +49.7(\frac{kJ}{mol}) \quad (1)$$

Water-gas shift reaction:

$$CO + H_2O \leftrightarrow CO_2 + H_2 \qquad \Delta = -41.2(\frac{kJ}{mol}) \quad (2)$$

and Methanol decomposition reaction:

$$CH_3OH \leftrightarrow CO + 2H_2 \qquad \Delta = +90.2(\frac{kJ}{mol}) \quad (3)$$

After the reforming process, the mixture turns into hydrogen-rich gas and is then directed to the fuel cell. While the fuel cell consumes a portion of the hydrogen and produce electricity, there are excess gas exiting the fuel cell as exhaust gas, which recirculated back to the burner to promote the overall system efficiency. The whole system operates in a high temperature at around 180 $°C$. To ensure that the system quickly reaches and maintains optimal operating temperature, an electric heater is installed within the burner to pre-heat it, which consumes additional electricity when operates. For the sake of simplification, an empirical model for the balance of plant (BoP) is adopted and is presented as can be found in [7].

In regards to the HT-PEM fuel cell, the output voltage drops due to the activation losses, ohmic losses, and concentration losses $V_{fc} = E_{oc} - V_{act} - V_{ohm}$, where E_{oc} is the open circuit voltage, V_{act} is the activation voltage, V_{ohm} represents the ohmic voltage [8].

$$\begin{cases} E_{oc} = K_c(1.229 + (T - 298)\frac{-44.43}{zF} + \frac{RT}{2F} ln(\frac{P_{H_2} P_{O_2}^{\frac{1}{2}}}{P_{H_2O}})) \\ V_{act} = \frac{NRT}{2\alpha F} ln(\frac{i_{fc}}{i_0}) \\ V_{ohm} = R_{ohm} i_{fc} \end{cases} \quad (4)$$

where K_c is the voltage constant at nominal operating condition, T is the fuel cell temperature in Kelvin, F stands for the Faraday constant, N is the number of cells, R is the ideal gas constant, P_{H_2}, P_{O_2}, and P_{H_2O} are the pressure of hydrogen, oxygen, and water, respectively. i_{fc} and i_0 represents the fuel cell current and reaction exchange current.

The polarization curve for the studied HT-PEMFC model is presented in Fig. 3 with parameters from manufacture in Table I.

C. Battery model

To address the inherently slow dynamic response of the fuel cell system and the fluctuated renewable energies, battery is adopted to provide auxiliary support for the microgrid. The battery model employed in this paper can be characterized

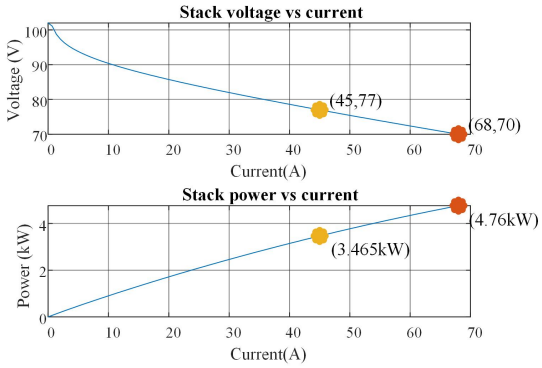

Fig. 3. Polarization curve

TABLE I
PARAMETERS FOR FC

Parameters	Symbol	Values
Nominal operating point	$[I_{nom}, V_{nom}]$	[45A, 77V]
Maximum operating point	$[I_{max}, V_{min}]$	[68A, 70V]
Open circuit point	$[0, E_{oc}]$	[0, 102V]
1A operating point	$[1, V_1]$	[1A, 99.8V]
Number of cells	N	120
Nominal LHV stack efficiency	η_{nom}	41%
Nominal operating temperature	T_{nom}	165 $^\circ C$
Nominal air flow rate	$V_{air_{nom}}$	500 L/min
Fuel pressure	$P_{fuel_{nom}}$	1.5
Air pressure	$P_{air_{nom}}$	1
Nominal composition	$[x_{nom}, y_{nom}]$	[99.95%, 21%]
Stack setting time	T_d	1s
Voltage variation	V_u	10%
Peak O2 utilization	$Uf_{O_{2peak}}$	80%[2]

by state of charge (SOC), voltage, internal resistance, and capacity. The model is defined by the following equations:

$$SOC_{bat} = SOC_{bat,0} - \int \frac{1}{3600 Q_{bat}} I_{bat} \tag{5}$$

where SOC_{bat} is the battery SOC, I_{bat} is the battery current, and Q_{bat} is the battery capacity. The terminal voltage of the battery is influenced by its SOC, and the empirical model for the terminal voltage as a function of SOC can be represented as in Fig. 4.

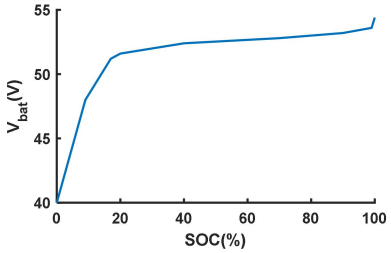

Fig. 4. Battery discharge curve

TABLE II
PARAMETERS FOR BATTERY

Parameters	Symbol	Values
Quantities	N_{bat}	1
Capacity	Q_{bat}	100 Ah
Internal resistance	R_{bat}	32 $m\Omega$
SOC limits	$SOC_{bat(min)}, SOC_{bat(max)}$	0.1,0.95

D. PV model

The output current of a PV module can be ideally calculated as [9]:

$$I_{pv} = I_{ph} - I_o(exp(\frac{V}{AN_sV_T}) - 1) \tag{6}$$

where I_{ph} is the photocurrent, I_o is the reverse saturation of the diode, V is the diode voltage, A is the ideality factor, N_s is the number of serial PV cells, and V_T is the thermal voltage.

E. Converter model

To achieve the energy management strategy, buck/boost DC/DC and AC/DC converters composed of controlled current source, controlled voltage source and LC filter is implemented in this paper to control the flow of energy from the FC, PV, and grid, respectively. For the purpose of rapid simulation, the average converter models are considered and shown in Fig. 5. And the voltage-current relationship between the source side and the bus side satisfies Equation 7 for the DC/DC converters and Equation 8 for the AC/DC converters, respectively.

$$\begin{cases} V_{in} = (\frac{1}{D_{dc/dc}} - 1)V_o \\ I_o = (\frac{1}{D_{dc/dc}} - 1)I_{in} \end{cases} \tag{7}$$

$$\begin{cases} V_o = rms(V_{a,in})D_{ac/dc} \\ I_o = rms(I_{a,in})\frac{1}{D_{ac/dc}} \end{cases} \tag{8}$$

$D_{dc/dc}$ and $D_{ac/dc}$ are duty ratio for the DC/DC converter and AC/DC converter, respectively.

III. CONTROLLER DESIGN

A decentralized control framework is developed for the studied microgid based on classic PI controller. The primary objective of this control system is to facilitate efficient primary power distribution among PV, fuel cell, battery, and the grid. The design ensures that the microgrid operates autonomously while having the ability to adapt its operation based on user's demand. To realize that, PI controller is the central of the control framework, which ensures the implementation of the developed state-based rules. Taking fuel cell as an example, the PI controller operates it either on constant power (CP) mode or constant voltage (CV) mode as can be found in Fig. 6. Each converter employs different controlling algorithm in a decentralized way. Due to the reason that the battery is connected directly to the DC bus, the DC bus voltage equals to the battery voltage and therefore highly related to the battery

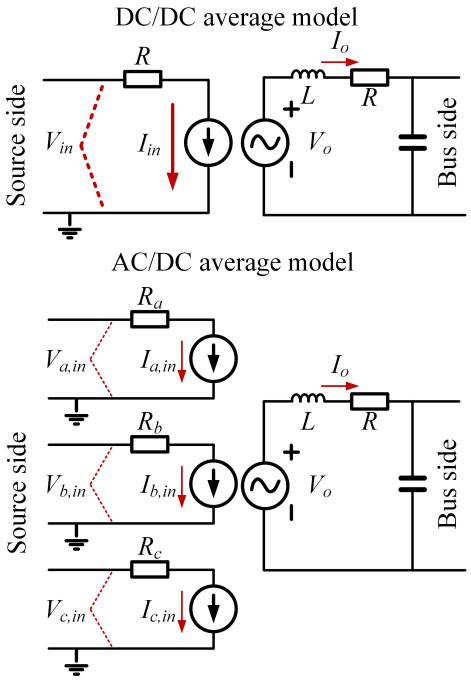

Fig. 5. Average converter model

State of Charge (SOC). By detecting the DC bus voltage, each controller adjusts the energy sector behavior automatically to realize the cooperation among them and to mitigate the risk of over-charging and over-discharging the battery. The design of each controller's control algorithm follows either a state-machine or a rule-based approach, as can be found in Fig. 7.

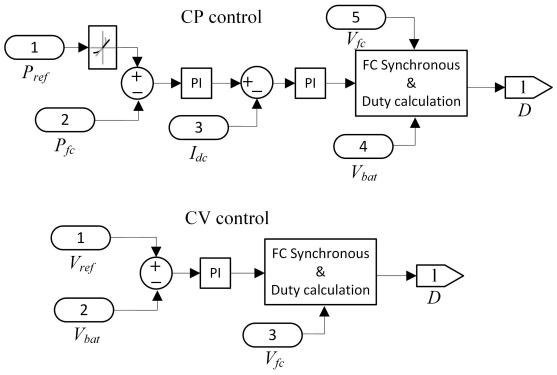

Fig. 6. Constant Power control and Constant Voltage control.

The controller for the automatic operation of the microgrid is based on the constant estimation of the system states, particularly, the battery voltage. The behavior of each energy sector is adjusted based on the comparison of the DC bus voltage against the operational voltage threshold specific to each sector. For instance in Fig. 7.a, The fuel cell system is turned on to constant power mode if the DC bus voltage falls below its start-up voltage ($V_{start,fc}$) for a predetermined duration (T_{delay}). And if DC bus voltage exceeds the upper

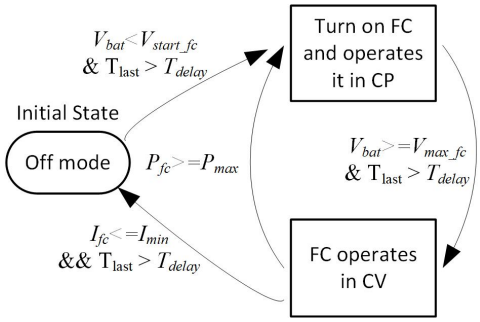

(a) Controlling algorithm for FC system

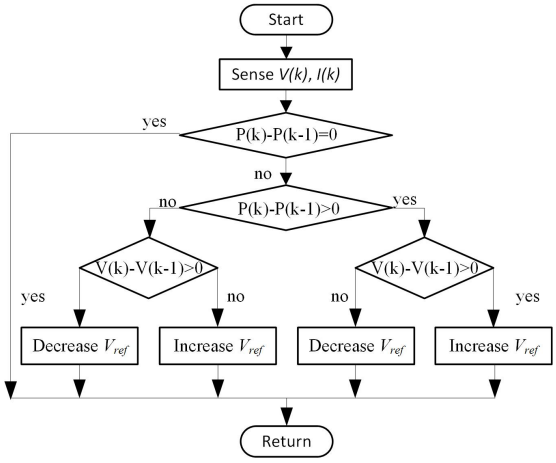

(b) Controlling algorithm for PV system

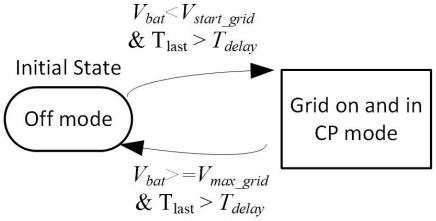

(c) Controlling algorithm for the grid system

Fig. 7. Automatic mode controller design for the microgid

threshold ($V_{max,fc}$), the fuel cell goes to constant voltage mode to prevent the overcharging of the battery. The fuel cell is automatically deactivated to prevent inefficient low-load operation if the output current goes below the minimum threshold (I_{min}), thereby optimizing operational efficiency. The control strategy for the PV system follows the MTTP control, as illustrated in Fig. 7.b [10], to fully take usage of the renewable energy potential. The electrical grid interfaces with the microgrid system via a Victron converter, as in Fig.8. However, this paper primarily concentrates on the DC aspects of the system. The grid connection is activated to draw constant power once the DC bus voltage reaches specified threshold values. This approach ensures the grid connection is activated only when there is insufficient energy support, thereby promoting a more grid-independent operation.

It's important to note that all threshold parameters as well

as the power reference values within the control system are adaptable, allowing for customization according to user demand or adjustments by a superior energy management system.

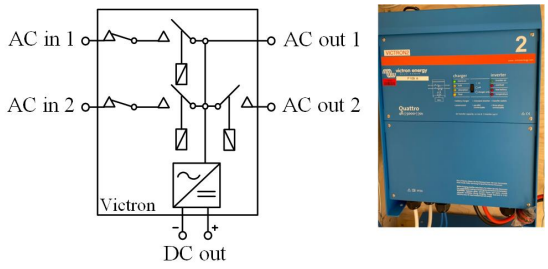

Fig. 8. Victron converter model

IV. Simulation Results

Simulation tests are carried out on MATLAB/Simulink R2022a to evaluate the performance of the developed system. The focus of the tests is to assess the system capability for stable operation in automatic mode and seamless transitions between different modes. The tests are specifically conducted within the context of a residential Internet of Things (IoT) house, targeting an energy consumption level of approximately 5kW. The general structure of the IoT house structure is as Fig.9.

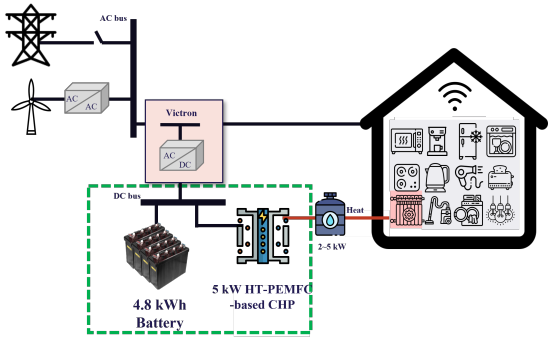

Fig. 9. The general structure of the IoT house

The methanol reformed HT-PEM fuel cell has great potential for combined heat and power (CHP) applications, offering the capability to generate heat in addition to electricity for residential uses. However, in this paper, we temporarily narrow our focus to the electrical generation aspect, specifically concentrating on the DC output of the system. This allows for a detailed exploration of the electrical performance and will eventually pave the way for future study of the combined electrical and thermal application.

The results of one case study under automatic mode are presented in Fig. 10, illustrating the dynamic responses of each energy source. It shall be noted that the fuel cell typically have a long start-up time of around 20 minutes, with the current gradually increasing to its normal operating level during this phase. However, to enhance simulation efficiency, the start-up time of the fuel cell was expedited to be 100 times faster than actual conditions, significantly reducing simulation time without compromising the quality of the results.

In this case study, the grid voltage threshold is set higher than that of the fuel cell, indicating a preference for utilizing grid power over the fuel cell in renewable energy shortage or when battery in low SOC conditions. However, this configuration can be adjusted based on different threshold settings, and this case study only gives one possibility. In this case study, initially, the load is supported only by the PV and battery. As the battery discharges, its voltage drops, reaching the grid's start-up threshold at around 20s, promoting grid connection to support the system and operating at constant power reference value. However, high load demand still leads to the continued discharging of the battery and a consequent decreasing in DC bus voltage. By approximately 80 seconds, the DC bus voltage falls to the fuel cell's start-up threshold, triggering the fuel cell to be turned on. After a startup period of about 10 seconds, the fuel cell operates in constant power mode at its maximum reference power output, resulting in battery recharge and thus increasing the DC bus voltage. Around 130 seconds, the DC bus voltage meets the fuel cell's lower voltage threshold, switching the fuel cell to constant voltage mode to prevent the battery overcharging. At around 240 seconds, a reduction in load causes the fuel cell current to drop below its minimum threshold, leading to the fuel cell to be turned off. Afterwards, the grid also disconnects because of the low load demand. The system repeats the similar behavior under the developed rules in the remaining simulations. Through the whole process, each energy sector autonomously coordinates operation based on DC bus voltage alone, without inter-sector communication. It can be seen from the simulation results that the system remains stable and effectively manages healthy battery SOC during load changes and PV irradiance changes.

V. Conclusion

A simplified yet efficient microgrid model with high penetration of renewable energies (PV, methanol reformed HT-PEM fuel cell system) is established in this paper, based on which a decentralized control framework is proposed. The decentralized control algorithm is developed based on PI controller, and is unique for each converter in respects to the characteristics of different energy sources. The proposed method can support the dynamic load changes, prevent overcharging and overcharging, realize automatic cooperation of the diverse energy sources and the seamless mode transition. In addition to it, the simplicity of the control algorithm and their real-time applicability make this framework a practical solution, and can be easily integrated with high-level energy management systems for enhanced performance, which will be developed in the future research.

References

[1] F. S. Al-Ismail, "Dc microgrid planning, operation, and control: A comprehensive review," *IEEE Access*, vol. 9, pp. 36 154–36 172, 2021.

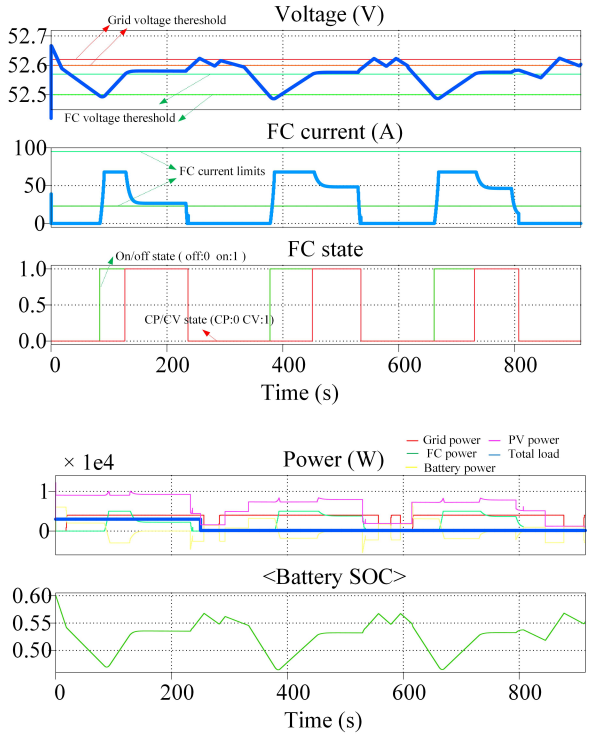

Fig. 10. System performance under one case study

[2] M. U. Shahid, M. M. Khan, K. Hashmi, R. Boudina, A. Khan, J. Yuning, and H. Tang, "Renewable energy source (res) based islanded dc microgrid with enhanced resilient control," *International Journal of Electrical Power & Energy Systems*, vol. 113, pp. 461–471, 2019.

[3] V. Suresh, N. Pachauri, and T. Vigneysh, "Decentralized control strategy for fuel cell/pv/bess based microgrid using modified fractional order pi controller," *International Journal of Hydrogen Energy*, vol. 46, no. 5, pp. 4417–4436, 2021.

[4] A. Bendib, A. Chouder, K. Kara, A. Kherbachi, S. Barkat, and W. Issa, "New modeling approach of secondary control layer for autonomous single-phase microgrids," *Journal of the Franklin Institute*, vol. 356, no. 13, pp. 6842–6874, 2019.

[5] P. Xie, J. M. Guerrero, S. Tan, N. Bazmohammadi, J. C. Vasquez, M. Mehrzadi, and Y. Al-Turki, "Optimization-based power and energy management system in shipboard microgrid: A review," *IEEE systems journal*, vol. 16, no. 1, pp. 578–590, 2021.

[6] J. Zhu, "Modelling of a packed-bed methanol steam reformer for ht-pem fuel cell applications," 2022.

[7] P. Xie, S. S. Araya, J. M. Guerrero, and J. C. Vasquez, "Dynamic modeling and control of high temperature pem fuel cell and battery system for electrical applications," in *IECON 2023-49th Annual Conference of the IEEE Industrial Electronics Society*. IEEE, 2023, pp. 1–6.

[8] G. L. Lopez, R. S. Rodriguez, V. M. Alvarado, J. Gomez-Aguilar, J. E. Mota, and C. Sandoval, "Hybrid pemfc-supercapacitor system: Modeling and energy management in energetic macroscopic representation," *Applied Energy*, vol. 205, pp. 1478–1494, 2017.

[9] H. Bellia, R. Youcef, and M. Fatima, "A detailed modeling of photovoltaic module using matlab," *NRIAG journal of astronomy and geophysics*, vol. 3, no. 1, pp. 53–61, 2014.

[10] M. A. Eltawil and Z. Zhao, "Mppt techniques for photovoltaic applications," *Renewable and sustainable energy reviews*, vol. 25, pp. 793–813, 2013.